UC Merced

UC Merced Previously Published Works

Title

Electronic Spectroscopy of Atomic Defects in Molybdenum Disulfide under Ambient Conditions

Permalink

https://escholarship.org/uc/item/75p2p872

Journal

ACS OMEGA

ISSN

2470-1343

Authors

Evans, Joshua R

Garibay, Diego A

Kuhls, Aiden N

et al.

Publication Date

2026-10-20

DOI

10.1021/acsomega.6c07020

Copyright Information

This work is made available under the terms of a Creative Commons Attribution License, available at https://creativecommons.org/licenses/by/4.0/

Peer reviewed

eScholarship.org Powered by the California Digital Library
University of California

ACS OMEGA

Open Access

This article is licensed under CC-BY-NC-ND 4.0

http://pubs.acs.org/journal/acsodf

Article

Electronic Spectroscopy of Atomic Defects in Molybdenum Disulfide under Ambient Conditions

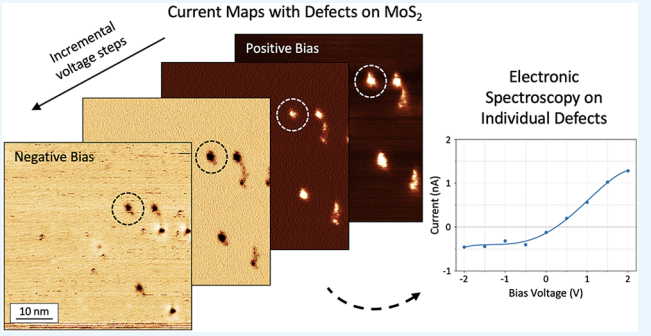
Joshua R. Evans, Diego A. Garibay, Aiden N. Kuhls, and Mehmet Z. Baykara*

Cite This: *ACS Omega* 2026, 11, 66942−66947

Read Online

ACCESS | Metrics & More | Article Recommendations | Supporting Information

ABSTRACT: We present results of electronic spectroscopy experiments performed on individual defects in the prototypical transition metal dichalcogenide (TMD) molybdenum disulfide (MoS_2) under ambient conditions by way of conductive atomic force microscopy (C-AFM). Data acquired in the form of consecutive, high-resolution current maps at various bias voltages allow the assessment of local conductivity and differential conductance as a function of bias voltage for individual defects, the effects of which range from single-atomic sites to several nanometers in lateral size. Characteristic behavior in spectroscopy data allows the categorization of observed defects into distinct groups and provides clues with regard to their chemical identities.



INTRODUCTION

Two-dimensional (2D) materials are being intensely studied since the discovery of the outstanding electrical properties exhibited by graphene in 2004.[1] 2D materials are attractive for a wide range of applications because of geometric reasons; their extreme thickness facilitates small-scale device designs. One important class of 2D materials is transition metal dichalcogenides (TMDs), which possess intriguing optoelectronic characteristics (e.g., direct and tunable bandgaps).[2]

An obstacle to the successful implementation of 2D TMDs in next-generation electronic devices is the presence of atomic-scale defects.[3] While certain atomic defects exist in TMDs naturally,[4] their introduction may also occur during laboratory synthesis.[5] Defects can reduce carrier mobility by acting as scatterers[6] and also modify the band gap.[7] Theory and experiments show that certain atomic defects can lead to an overall increase in electronic heterogeneity via in-gap states.[8] The heterogeneous spatial distribution of atomic defects may also lead to inconsistencies and reliability concerns in batch-fabricated devices.[9]

The discussion above highlights the need for precise defect characterization in 2D TMDs as a crucial step in their implementation in applications. Such information can help refine synthesis processes to control defect types and densities.[10] Multiple characterization techniques exist that can probe atomic defects in 2D TMDs. Scanning tunneling microscopy (STM) is the most conventional one, together with scanning tunneling spectroscopy (STS), which reveals the electronic density of states (DOS) associated with defective sites, facilitating defect identification based on characteristic changes in DOS.[5,11]

A critical limitation associated with STM is the requirement of performing experiments under ultrahigh-vacuum (UHV) conditions, due to the necessity of molecularly clean surfaces. This leads to complications including low throughput due to extended sample preparation and measurement procedures. The UHV environment is also not representative of the typical conditions under which devices based on 2D TMDs operate, limiting the relevance of the results for practical applications.

Recently, atomic-resolution imaging was achieved under ambient conditions via conductive atomic force microscopy (C-AFM).[12,13] Specifically, it was demonstrated that C-AFM can image the same atomic defects as STM on 2D TMDs.[14] On the other hand, C-AFM images alone do not provide information on the chemical identity of the defects, complicating data interpretation. While measurements of current (I) as a function of bias voltage (V), reminiscent of STS, may indeed be performed by C-AFM,[15,16] this approach is not suitable for studying the electrical characteristics of atomic defects because of problems associated with thermal drift. Specifically, lateral misalignments between the tip and the sample result in significantly reduced levels of confidence in assigning the recorded electronic signatures to specific defects.

Motivated in this fashion, we present here a C-AFM-based approach enabling the electronic spectroscopy of individual atomic defects under ambient conditions. Our methodology, applied to exfoliated flakes of the prototypical TMD

Received: June 16, 2026
Revised: September 24, 2026
Accepted: October 6, 2026
Published: October 20, 2026



ACS Publications

© 2026 The Authors. Published by American Chemical Society

Downloaded from pubs.acs.org/acsodf/article-pdf/11/43/66942/6892116/acsomega.6c07020.pdf by UNIV OF CALIFORNIA MERCED user on 03 November 2026

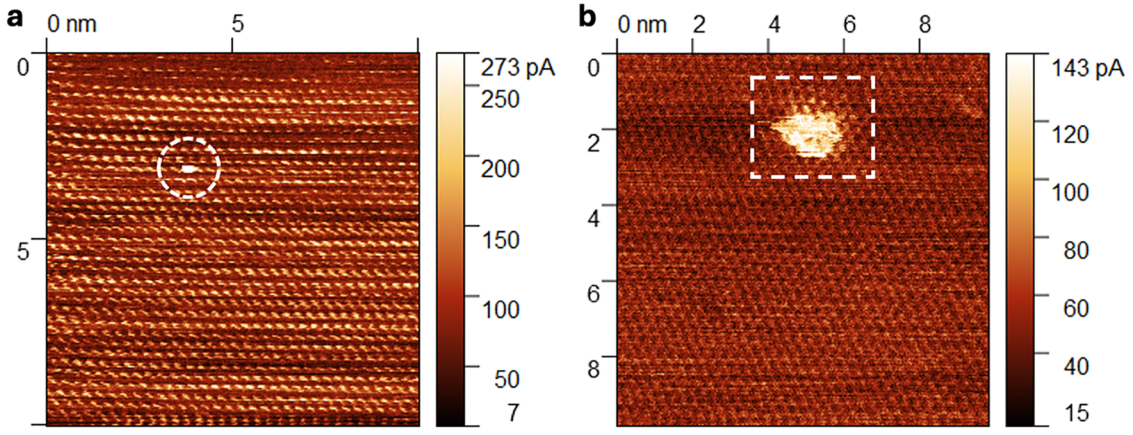


Figure 1. (a) Current map comprising a point defect (highlighted by the dashed white circle) on the MoS_2 surface. Bias voltage: +2.5 V. (b) Current map showing a larger defect spanning multiple lattice sites (highlighted by the dashed white rectangle). Bias voltage: +2 V.

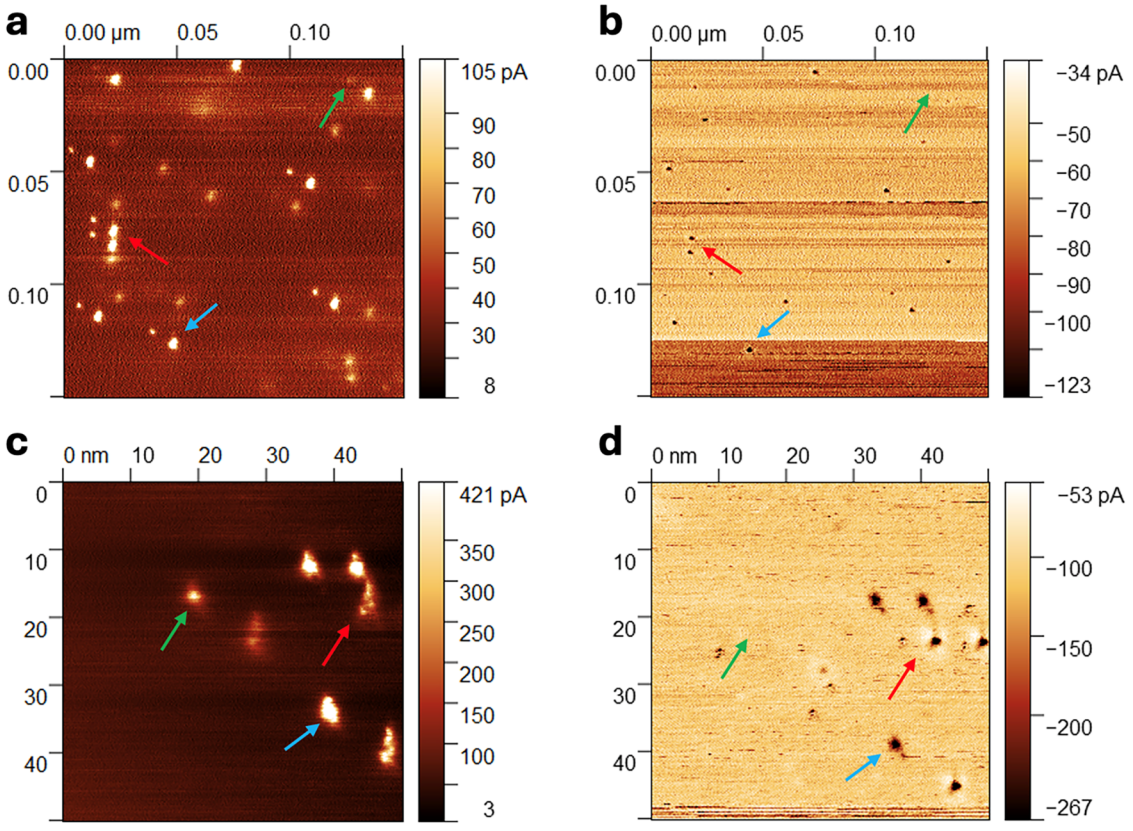


Figure 2. Pairs of current maps recorded at different bias voltages on MoS_2. The top row shows two 150 × 150 nm^2 current maps on the same area, recorded at two different bias voltages: (a) +2 V, and (b) −2 V. While some defects enhance current at both bias polarities (blue and red arrows), others are not detectable at negative bias voltage (green arrow). The bottom row shows two 50 × 50 nm^2 current maps, recorded at (c) +2 V and (d) −2 V. Defects exhibit different spatial morphologies at opposing polarities (blue and red arrows), while a particular defect is again not detectable at negative bias voltage (green arrow).

molybdenum disulfide (MoS_2), allows us to categorize observed defects into various groups based on their bias-voltage-dependent electronic behavior and provides clues with regard to their identities.

RESULTS AND DISCUSSION

Figure 1 demonstrates the capability of C-AFM to image defects of various sizes on MoS_2 under ambient conditions. Specifically, Figure 1a comprises a 10 × 10 nm^2, atomic-resolution current map where a point (i.e., single-atomic) defect can be observed, locally enhancing the conductivity. Such single-atomic, current-enhancing defects were previously observed in MoS_2 and attributed to subsurface/buried substitutions of a S atom, potentially by O.[5,17] The capability to image single-atomic defects fulfills the criterion of *true* atomic-resolution imaging.[12] The 10 × 10 nm^2 current map presented in Figure 1b shows a current-enhancing defect spanning multiple lattice sites over a lateral distance of ∼1.5 nm. The point defect in Figure 1a proves useful for characterizing the thermal drift between the tip and the sample. By following the position of the point defect over

https://doi.org/10.1021/acsomega.6c07020
ACS Omega 2026, 11, 66942−66947

Downloaded from pubs.acs.org/acsodf/article-pdf/11/43/66942/6892216/acsomega.6c07020.pdf by UNIV OF CALIFORNIA MERCED user on 03 November 2026

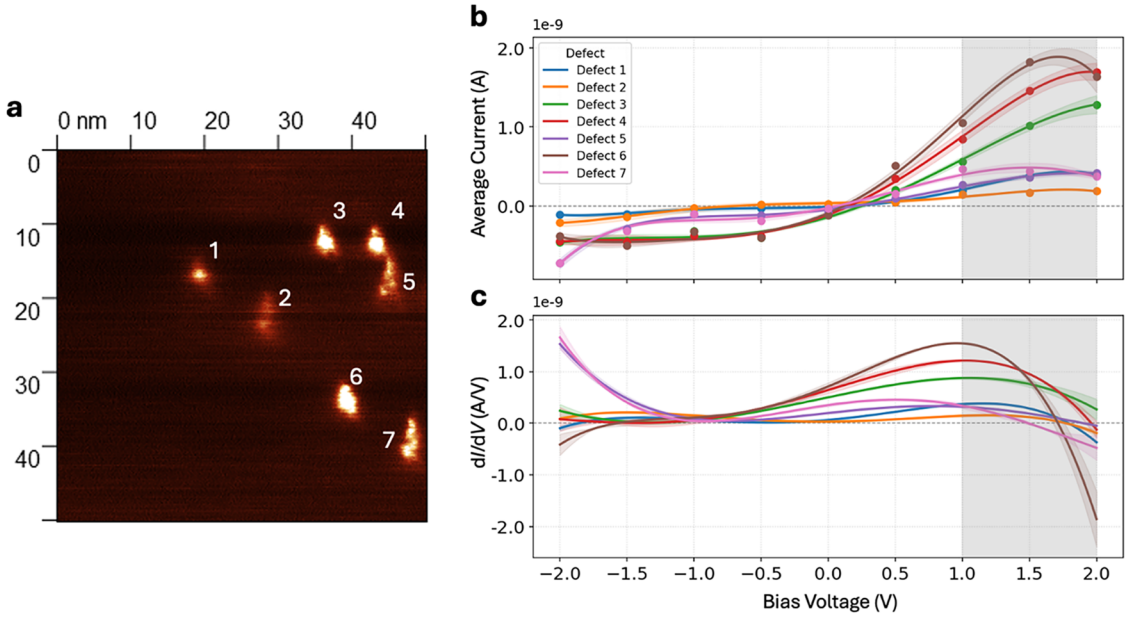


Figure 3. (a) Current map of defects on MoS_2. Bias voltage: +2 V. (b) Average current values plotted as a function of the bias voltage, for each of the seven defects observed in (a). Each set of points is fitted with a 5th-degree polynomial, resulting in a characteristic, continuous $I-V$ curve. (c) Derivative of each fitted curve from (b), producing the $dI/dV-V$ curve for all observed defects in (a). The shaded area in (b) and (c) highlights the potential occurrence of a tip change, causing an unexpected drop in slope. Please note that the current data in (b) are in the (sub-)nA range.

consecutive scans, the drift rate was estimated to be ∼6 Å/min (i.e., ∼0.1 Å/s)—sufficiently low for tracking the same defect (or a group of defects) over multiple minutes (please see the Supporting Information).

While small current maps are useful for characterizing the atomic structure of individual defects, larger images are required to make conclusions about their variety and spatial density. As such, additional images were taken on MoS_2 at larger scan sizes, which revealed the presence of various defects that perturb local conductivity (Figure 2). Defects were found to differ in terms of their lateral size, as well as their spatial morphology, and notably, their bias-voltage-dependent electronic behavior. The latter point is illustrated by pairs of current maps recorded over the same area at two different bias voltages (Figure 2a–d). While some defects enhance conductivity at both positive and negative bias voltages, others are only detectable at one bias polarity. Moreover, the spatial, defect-specific morphology of electronic perturbation changes at different bias polarities (Figure 2c,d). These observations open the avenue of using voltage-dependent electronic behavior as the "fingerprint" for classifying defects in 2D TMDs.

To study the electronic behavior of individual defects, electronic spectroscopy needs to be performed in the form of $I-V$ curves, from which $dI/dV-V$ (differential conductance) behavior can be extracted. To overcome issues with thermal drift, we developed a new methodology for data collection named "discrete $I-V$ spectroscopy". In particular, the technique operates by recording sets of multiple, complete current maps on an area with the defect(s) of interest at discrete bias voltages. While the spread of data points in terms of bias voltage is significantly less dense compared to conventional $I-V$ spectroscopy, notable benefits of the new technique are the following: (i) no uncertainty in assigning the recorded data to specific locations on the surface, (ii) the ability to characterize multiple defects simultaneously within the same scanning frame, and (iii) the ability to track the spatial morphology of electronic perturbations induced by the defects. While thermal drift certainly takes place during the recording of individual current maps, the fast scan rate of 15.62 Hz is sufficiently high to overcome any appreciable effect of thermal drift (which is on the order of only ∼0.1 Å/s), as a typical individual defect is imaged over a duration of <1 s.

In order to assign current values to individual defects, we fit a 2D Gaussian surface to an elliptical area around the defect, whereby the amplitude of the surface corresponds to the current value associated with that defect. The 2D Gaussian surface fitting described here produces more accurate current values compared to manual fitting of 1D Gaussian lines on defects (please see the Supporting Information). This is because multiple line profiles are collected along the span of an individual defect in the 1D Gaussian line-fitting approach, whereby the amplitudes extracted from each line are averaged to obtain a characteristic current value. As a significant number of line profiles do not go over the highest current region (the "peak") of the defect, the resulting average current value is attenuated with respect to the peak value. The fitting procedure is repeated for all images recorded at a given bias voltage; the averaged amplitude value is then assigned to that defect as its characteristic current. Replicating the process at other voltage values then provides bias-voltage-dependent current data ($I-V$) for all defects in a scan frame. Polynomial fits to the $I-V$ data are then produced, the slopes of which are calculated to extract defect-specific $dI/dV-V$ information. For this purpose, fifth-degree polynomial fits are generally preferred, as sixth (and higher) degree fits are observed to "overfit" the data and thus result in individual outliers influencing the overall trend disproportionately. A comparison of current data acquired at sequentially and randomly ordered bias voltage values demonstrates that temporal effects such as gradual charging do not influence the recorded data (please see the Supporting Information).

Following the procedure described above, we performed electronic spectroscopy on all defects observed in Figure 2(c,d).

https://doi.org/10.1021/acsomega.6c07020
ACS Omega 2026, 11, 66942−66947

Downloaded from pubs.acs.org/acsodf/article-pdf/11/43/66942/6892216/acsomega.6c07020.pdf by UNIV OF CALIFORNIA MERCED user on 03 November 2026

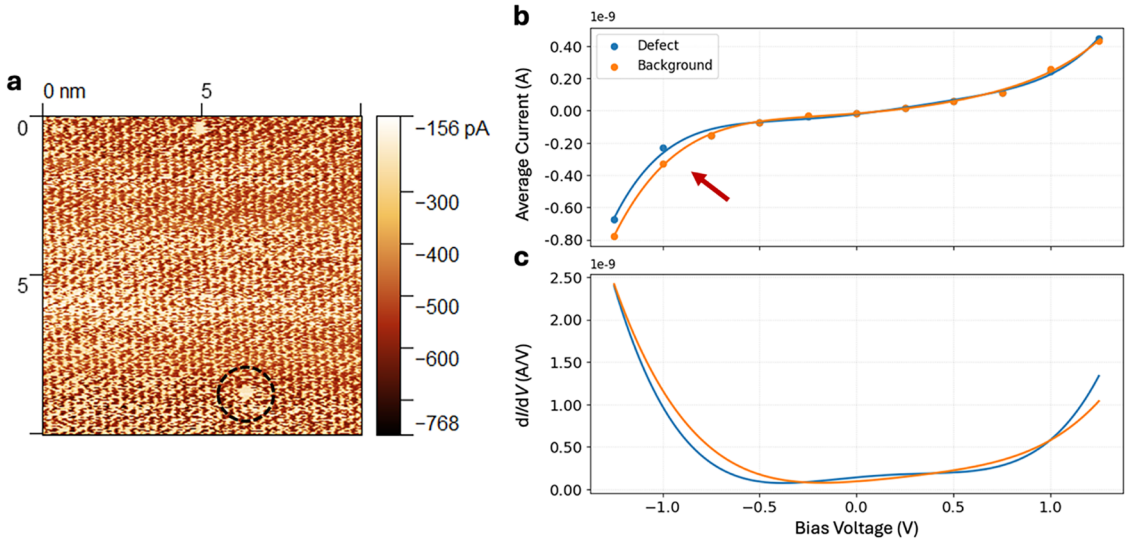


Figure 4. (a) A 10×10 nm^2 current map on MoS_2 imaged at a bias voltage of −1 V, where two point defects are detected. (b) Average current plotted as a function of the bias voltage for the point defect highlighted by the dashed black circle in (a) (blue), as well as a nondefective (i.e., background) region in its vicinity (orange). The two sets of points are fitted with 5th-degree polynomials. A deviation of current on the defect from the background signal is detected at increasingly negative voltages (red arrow). (c) dI/dV−V curves for the defect (blue) and the background (orange). Please note that the current data in (b) are in the (sub-)nA range.

This was done by way of images collected between bias voltages of +2 V and −2 V, in 0.5 V increments (with 5 images per bias voltage value), the results of which are presented in Figure 3. Studying the behavior summarized in Figure 3, we can categorize the observed defects into three different groups. Defects 1 and 2 (Group 1) weakly enhance the conductivity at both positive and negative bias voltages, with a relatively flat dI/dV profile across the voltage range. On the other hand, defects 3, 4, and 6 (Group 2) exhibit a prominent increase in conductivity with increasing bias voltage in the positive region, accompanied by relatively weak and bias-independent enhancement of current at bias voltages of −0.5 V and below. Defects 5 and 7 form the last set (Group 3), with their characteristic behavior being a prominent increase in dI/dV at increasingly negative bias voltages and otherwise similar behavior to group 1 defects.

It should be noted that an unexpected drop in current slopes happens for the majority of defects at/around a bias voltage of +1 V (shaded regions in Figure 3b,c, in some cases into the negative regime), which potentially points to a gradual change in the tip−sample contact. On the other hand, characteristic features such as a prominent increase in current at increasingly negative bias voltages only happen for a certain set of defects (Group 3), allowing their robust assignment as defect-specific changes in electronic properties.

It is particularly important to highlight that the grouping of defects performed in this fashion is strongly supported by the morphological features observable from the current maps. Specifically, the spatial shape of defects assigned to each group is consistent with each other, as one can see in the current map presented in Figure 3a. This provides further validation for the applicability of discrete I−V spectroscopy for defect categorization.

Comparison of electronic spectroscopy results with existing studies in the literature allows making predictions about the chemical identity of the defects. In particular, the relatively flat dI/dV plots approaching 0 for the majority of defects in the negative voltage regime (except for Group 3) are indicative of defect-induced band bending or charge trapping mechanisms that were previously observed in STM-derived differential conductance (dI/dV) curves associated with transition metal substitutions.[4] Another key piece of information regarding the chemical identity of the defects is gathered by comparing their character in terms of current-enhancing vs current-attenuating at opposing bias voltage polarities. In particular, all defects observed in Figure 3 enhance current locally for both positive and negative bias voltages. This polarity-independent, current-enhancing character exhibited by defects support their assignment as individual, noncharged (i.e., neutral) transition metal substitutions (or clusters thereof), in alignment with studies performed by Bampoulis et al.[18] and Dunn et al.[17] While additional factors such as the lateral extent (several nanometers) and the spatial density ($\sim$1.5−3.0 $\times$ 10^{11} cm^{-2}) of defects observed in Figures 2 and 3 further support their assignment as transition metal substitutions,[18] additional details in the data allow more distinctions to be made between the defects. Specifically, defects in Group 3 exhibit enhanced current and differential conductance at increasingly negative bias voltages, as opposed to others. This behavior points to a local abundance of donor states, indicative of n-type doping.[19] On the other hand, the significant increase in current and differential conductance at increasingly positive bias voltages for Group 2 defects is indicative of p-type doping.[20] Finally, the effect of Group 1 defects on the differential conductance is less noticeable than Group 2 and 3, potentially pointing toward a different transition metal dopant than Groups 2 and 3. It is important to note that the conclusions made here with regard to the chemical identities of the defects are specific to MoS_2 flakes exfoliated from flux-grown bulk crystals, and samples fabricated via other methods (such as chemical vapor deposition (CVD)) may predominantly feature other types of defects.

The approach described here can also be extended to the study of single-atomic defects in order to elucidate their bias-voltage-dependent behavior. The results of such an effort are presented in Figure 4, where two single-atomic defects are detected in a small-scale (10×10 nm^2) current scan on MoS_2. The defects locally attenuate the current in comparison to their

https://doi.org/10.1021/acsomega.6c07020
ACS Omega 2026, 11, 66942−66947

Downloaded from pubs.acs.org/acsodf/article-pdf/11/43/66942/6892216/acsomega.6c07020.pdf by UNIV OF CALIFORNIA MERCED user on 03 November 2026

surroundings, at both bias polarities. Tracking the currents on a particular defect (Figure 4a) as a function of bias voltage in a range of −1.25 V to +1.25 V then allows the extraction of characteristic $I-V$ behavior (Figure 4b). Comparison of $I-V$ behavior with a nondefective location in the vicinity of the defect reveals close overlap in the positive voltage range (i.e., toward the conduction band), whereby the current detected over the negative voltage range (i.e., toward the valence band) slightly deviates from the nondefective region. Moreover, no significant distortions (e.g., in the form of in-gap states) are induced by the point defect in differential conductance measurements (Figure 4c).

There is considerable debate in the literature regarding the identity of point defects observed in TMDs. While S vacancies have been conventionally considered as the primary candidates in samples grown via CVD,[21] recent STM/STS and DFT work have pointed toward O atoms substituting S sites at or near the surface as the predominant point defect in flux-grown TMDs.[5] Unlike O substitutions, S vacancies are expected to result in in-gap states close to the conduction band minimum in MoS_2.[22] On the other hand, O substitutions do not induce in-gap states and $dI/dV-V$ spectra remain mostly unperturbed with slight modifications near the valence band maximum.[5,11] These characteristics are in strong alignment with the data presented in Figure 4. It may be argued that the relatively sparse density of data points in our measurement (with a spacing of 0.25 V) may have potentially prevented the observation of an in-gap state. On the other hand, the calculated density of point defects ($\sim 2.0 \times 10^{12}$ cm^{-2}, which is in accordance with the literature[23]) and their current-attenuating character toward the valence band are additional factors that are suggestive of O substitutions of S.

CONCLUSIONS

We presented here a methodology that enables the extraction of local electronic characteristics associated with individual atomic defects in the prototypical TMD, MoS_2. Our methodology notably works under ambient conditions with virtually no sample preparation and thus much higher throughput than UHV-based methods such as STM. The data additionally allow the categorization of defects based on signatures of local electronic behavior. The method described here is not restricted to TMDs and can be expanded to the study of other electronic and quantum materials under application-relevant (i.e., ambient) conditions.

METHODS

For the experiments presented here, bulk, flux-grown MoS_2 crystals were obtained commercially (2D Semiconductors) and mechanically exfoliated via the adhesive tape method[1] onto conductive substrates in the form of gold-coated silicon wafers (*Substrata*, gold thickness: 50 nm). C-AFM imaging and spectroscopy experiments were performed with a commercial instrument (Cypher VRS, *Asylum Research, Oxford Instruments*). Conductive-diamond-coated tips (CDT-CONTR, *Nanosensors* and AD-2.8-AS, *Adama*) were used for imaging, in alignment with previous work.[12] Atomic resolution is achieved using high-speed scanning (at a scanning frequency of 15.62 Hz), which counteracts the effects of thermal drift and water meniscus aging at the tip−sample junction.[24] Experiments are performed under ambient conditions (temperature range: 22−23 °C; relative humidity range: 20−50%). The bias voltage is applied to the sample. It should be noted that the method of atomic-resolution C-AFM under ambient conditions is new,[12] and there is considerable debate with regard to the physical mechanisms of current conduction at the tip−sample junction in the presence of adsorbed contaminants. As such, potential effects such as barrier-like junctions at the interface cannot be completely ruled out. Having said this, the spectroscopic information collected over defects presents trends with intriguing similarities to UHV-based STM data presented in the literature.[4,11]

ASSOCIATED CONTENT

Supporting Information

The Supporting Information is available free of charge at https://pubs.acs.org/doi/10.1021/acsomega.6c07020.

Imaging of a point defect during discrete $I-V$ spectroscopy (MP4)

Characterization of thermal drift; 1D vs 2D Gaussian fitting; and sequentially ordered vs randomly ordered data collection (PDF)

AUTHOR INFORMATION

Corresponding Author

Mehmet Z. Baykara − *Department of Mechanical and Aerospace Engineering, University of California Merced, Merced, California 95343, United States;* orcid.org/0000-0002-0278-6022; Email: mehmet.baykara@ucmerced.edu

Authors

Joshua R. Evans − *Department of Materials Science and Engineering, University of California Merced, Merced, California 95343, United States*

Diego A. Garibay − *Department of Mechanical and Aerospace Engineering, University of California Merced, Merced, California 95343, United States*

Aiden N. Kuhls − *Department of Mechanical and Aerospace Engineering, University of California Merced, Merced, California 95343, United States*

Complete contact information is available at: https://pubs.acs.org/10.1021/acsomega.6c07020

Author Contributions

M.Z.B. conceived the project. J.R.E., D.A.G., and A.N.K. performed the C-AFM experiments. J.R.E. performed the data analysis. All authors participated in the interpretation of the results and the writing of the manuscript.

Notes

The authors declare no competing financial interest.

ACKNOWLEDGMENTS

This work was supported by the VISION (Venture for Innovation in Self-assembly and Integration of Optoelectronic Nanostructures) Center at the University of California, Merced, which is funded by the Partnerships for Research and Education in Materials (PREM) program of the National Science Foundation (NSF) via Award No. 2425230. We acknowledge fruitful discussions with Prof. Matthew Rosenberger at the University of Notre Dame.

REFERENCES

(1) Novoselov, K. S.; Geim, A. K.; Morozov, S. V.; Jiang, D.; Zhang, Y.; Dubonos, S. V.; Grigorieva, I. V.; Firsov, A. A. Electric field effect in atomically thin carbon films. *Science* **2004**, *306* (5696), 666−669.

(2) Manzeli, S.; Ovchinnikov, D.; Pasquier, D.; Yazyev, O.; Kis, A. 2D transition metal dichalcogenides. *Nat. Rev. Mater.* **2017**, *2* (8), No. 17033.

Downloaded from pubs.acs.org/acsodf/article-pdf/11/43/66942/6892116/acsomega.6c07020.pdf by UNIV OF CALIFORNIA MERCED user on 03 November 2026

(3) Krasheninnikov, A. V.; Batzill, M.; Delenda, A.; Drndic, M.; Ewels, C.; Franke, K.; Ghorbani-Asl, M.; Holleitner, A.; Jorio, A.; Kaiser, U.; et al. Defects and defect-mediated engineering of two-dimensional materials: challenges and open questions. *Beilstein J. Nanotechnol.* **2026**, *17*, 454−488.
(4) Addou, R.; Colombo, L.; Wallace, R. M. Surface Defects on Natural MoS_2. *ACS Appl. Mater. Interfaces* **2015**, *7* (22), 11921−11929.
(5) Holbrook, M.; Holtzman, L.; Hou, B.; Nashabeh, L.; Qiu, D.; Barmak, K.; Pasupathy, A.; Hone, J. Revealing Substitutional Oxygen as the Dominant Defect in Flux-Grown Transition Metal Diselenides. *Nano Lett.* **2025**, *25* (37), 13795−13801.
(6) Sun, J.; Passacantando, M.; Palummo, M.; Nardone, M.; Kaasbjerg, K.; Grillo, A.; Di Bartolomeo, A.; Caridad, J.; Camilli, L. Impact of Impurities on the Electrical Conduction of Anisotropic Two-Dimensional Materials. *Phys. Rev. Appl.* **2020**, *13* (4), No. 044063.
(7) Liang, Q.; Zhang, Q.; Zhao, X.; Liu, M.; Wee, A. Defect Engineering of Two-Dimensional Transition-Metal Dichalcogenides: Applications, Challenges, and Opportunities. *ACS Nano* **2021**, *15* (2), 2165−2181.
(8) Kumral, B.; Barri, N.; Demingos, P.; Adabasi, G.; Grishko, A.; Wang, G.; Kawase, J.; Onodera, M.; Machida, T.; Baykara, M.; et al. Mechanically reliable and electronically uniform monolayer MoS_2 by passivation and defect healing. *Nat. Commun.* **2025**, *16* (1), No. 7105.
(9) Yang, Y.; Xu, K.; Pena, T.; Neilson, K.; Zheng, X.; Hoang, A.; Yang, K.; Hennighausen, Z.; Zhang, T.; Holtzman, L.; et al. Nondestructive Atomic Defect Quantification of Two-Dimensional Materials and Devices. *ACS Appl. Mater. Interfaces* **2026**, *18* (6), 10161−10170.
(10) Liu, S.; Liu, Y.; Holtzman, L.; Li, B.; Holbrook, M.; Pack, J.; Taniguchi, T.; Watanabe, K.; Dean, C.; Pasupathy, A.; et al. Two-Step Flux Synthesis of Ultrapure Transition-Metal Dichalcogenides. *ACS Nano* **2023**, *17* (17), 16587−16596.
(11) Barja, S.; Refaely-Abramson, S.; Schuler, B.; Qiu, D.; Pulkin, A.; Wickenburg, S.; Ryu, H.; Ugeda, M.; Kastl, C.; Chen, C.; et al. Identifying substitutional oxygen as a prolific point defect in monolayer transition metal dichalcogenides. *Nat. Commun.* **2019**, *10*, No. 3382.
(12) Sumaiya, S. A.; Liu, J.; Baykara, M. Z. True Atomic-Resolution Surface Imaging and Manipulation under Ambient Conditions via Conductive Atomic Force Microscopy. *ACS Nano* **2022**, *16* (12), 20086−20093.
(13) Sumaiya, S. A.; Baykara, M. Atomic-scale imaging and spectroscopy via scanning probe microscopy: An overview. *J. Vac. Sci. Technol. B* **2023**, *41*, No. 060802.
(14) Xu, K.; Holbrook, M.; Holtzman, L.; Pasupathy, A.; Barmak, K.; Hone, J.; Rosenberger, M. Validating the Use of Conductive Atomic Force Microscopy for Defect Quantification in 2D Materials. *ACS Nano* **2023**, *17* (24), 24743−24752.
(15) Adabasi, G.; Kumar, S.; Okay, E.; Evans, J.; Atli, E.; Ancheta, J.; Buke, G.; Martini, A.; Baykara, M. Strain-Modulated Conductivity and Work Function on Thin Crystals of Mo_2C. *ACS Appl. Nano Mater.* **2025**, *8* (41), 19810−19817.
(16) Adabasi, G.; Baykara, M. Scanning probe microscopy of MXenes: state of the art and prospects. *Nano Futures* **2025**, *9* (3), No. 032501.
(17) Dunn, E. J.; Robson, A.; Young, R.; Jarvis, S. Single atom chemical identification of TMD defects in ambient conditions. *Nanotechnology* **2026**, *37* (13), No. 135705.
(18) Bampoulis, P.; van Bremen, R.; Yao, Q.; Poelsema, B.; Zandvliet, H.; Sotthewes, K. Defect Dominated Charge Transport and Fermi Level Pinning in MoS_2/Metal Contacts. *ACS Appl. Mater. Interfaces* **2017**, *9* (22), 19278−19286.
(19) Murata, H.; Kataoka, K.; Koma, A. Scanning tunneling microscope images of locally modulated structures in layered materials, $MoS_2(0001)$ and $MoSe_2(0001)$, induced by impurity atoms. *Surf. Sci.* **2001**, *478* (3), 131−144.
(20) Lu, S.-C.; Leburton, J. Electronic structures of defects and magnetic impurities in MoS_2 monolayers. *Nanoscale Res. Lett.* **2014**, *9*, No. 676.
(21) Hong, J.; Hu, Z.; Probert, M.; Li, K.; Lv, D.; Yang, X.; Gu, L.; Mao, N.; Feng, Q.; Xie, L.; et al. Exploring atomic defects in molybdenum disulphide monolayers. *Nat. Commun.* **2015**, *6*, No. 6293.
(22) Santosh, K.; Longo, R.; Addou, R.; Wallace, R.; Cho, K. Impact of intrinsic atomic defects on the electronic structure of MoS_2 monolayers. *Nanotechnology* **2014**, *25* (37), No. 375703.
(23) Trainer, D. J.; Nieminen, J.; Bobba, F.; Wang, B.; Xi, X.; Bansil, A.; Iavarone, M. Visualization of defect induced in-gap states in monolayer MoS_2. *NPJ 2D Mater. Appl.* **2022**, *6* (1), No. 13.
(24) Yuan, Y.; Lanza, M. The Effect of Relative Humidity in Conductive Atomic Force Microscopy. *Adv. Mater.* **2024**, *36* (51), No. 2405932.

Downloaded from pubs.acs.org/acsodf/article-pdf/11/43/66942/6892216/acsomega.6c07020.pdf by UNIV OF CALIFORNIA MERCED user on 03 November 2026

https://doi.org/10.1021/acsomega.6c07020
ACS Omega 2026, 11, 66942−66947